Chapter 8

Multicell Design for Concentrated Photovoltaic (CPV) Module

Muhammad Burhan,
Muhammad Wakil Shahzad and Kim Choon Ng

Additional information is available at the end of the chapter

http://dx.doi.org/10.5772/intechopen.78000

Abstract

Despite its highest efficiency, concentrated photovoltaic (CPV) technology is still finding its way into the current photovoltaic market which is saturated with conventional flat-plate photovoltaic systems. CPV systems have a great performance potential as they utilize third-generation multi-junction solar cells. In the CPV system, the main aspect is its concentrating assembly design which affects not only its overall performance but also its operation and fabrication. Conventional CPV design targets to use individual solar concentrator for each solar cell. The main motivation of this chapter is to propose a novel concentrating assembly design for CPV that is able to handle multiple solar cells, without affecting their size, using single solar concentrator. Such proposed design, named as multicell concentrating assembly (MCA), will not only reduce the assembly efforts during CPV module fabrication, but it will also lower the overall system cost with simplified design. In this chapter, a detailed design methodology of multicell concentrating assembly (MCA) for CPV module is presented and developed with complete verification through ray tracing simulation and field experimentation.

Keywords: novel concentrator, homogenizer, CPV, concentrator photovoltaic, multi-junction solar cell

1. Introduction

Due to dependency of global energy need on fossil fuels, the global warming situation is hitting to an alarming level with record amount of greenhouse gas emissions. Under such circumstances, renewable energy resources are seen to be able to provide sustainable energy source to

meet global energy needs [1–4]. However, solar energy, being the energy source with the highest energy potential [5–7], can provide a sustainable source of future primary energy supply if captured with high efficiency and simple configuration. Photovoltaic system provides the most simple configuration to convert solar energy into high-grade energy form, i.e., electricity. However, in the current photovoltaic market with 99% share of single-junction solar cells, the multi-junction solar cells (MJCs) have yet to exploit their potential of the highest solar energy conversion efficiency. This is due to the fact that the multi-junction solar cell (MJC) can respond to a full spectrum of solar radiation, with less loss and as a result higher efficiency [8–12]. On the other hand, due to their high material cost, MJCs are not available in the form of flat-plate panels like conventional single-junction solar cells. But rather, they are utilized in the form of concentrated photovoltaic (CPV) system where low-cost solar concentrators concentrate solar radiations onto the small area of solar cell material, thereby reducing the use of expensive solar cell material by 500 or 1000 times [13–17]. This is possible because MJC can withstand high concentrations. However, all of the commercial CPV modules, available hitherto, can only accommodate single solar cell per concentrator [18, 19]. Such conventional system requires increased assembly efforts. Therefore, by keeping the cell size same, this chapter discusses a novel CPV module design which can accommodate multiple MJCs with single solar concentrator.

2. Multicell concentrating assembly (MCA)

The simple concept of proposed multicell concentrating assembly (MCA) is shown in **Figure 1**, for novel CPV module design. The concentrating assembly is based upon a multi-leg homogenizer concept which allows the rays, collected from specially arranged pair of solar concentrators, to be uniformly distributed and transferred to four MJCs. In a simple form, received parallel solar radiations are transformed into a concentrated collimated beam, with the help of a pair of parabolic concentrators which are arranged in Cassegrain form. The concentrated collimated beam strikes at the inlet aperture of multi-leg homogenizer where it is uniformly split and distributed among MJCs, placed at the four outlet apertures of the homogenizer. In conventional CPV module design, the homogenizer is placed to accommodate the tracking errors

Figure 1. Schematic of novel multicell concentrating assembly (MCA) for CPV module.

associated with the two axis solar tracking, during CPV operation. However, in the proposed novel multicell concentrating assembly (MCA) design, the homogenizer not only serves as part of conventional homogenizer, but it also helps to split the collimated beam received from a pair of parabolic concentrators. Such ray splitting is achieved because of the fact that the collimated beam, at the inlet aperture of homogenizer, makes an area concentration unlike conventional concentrating assembly design in which point concentration is achieved. By using the concept of concentrator photovoltaics (CPV), the expensive semiconductor multi-junction solar cell material was replaced with cheap solar concentrators. However, with the proposed multicell concentrating assembly design, the cost and assembly efforts of CPV modules will be reduced as a less number of solar concentrators will be needed for same capacity of the system.

3. Theoretical design of MCA

The theoretical design of proposed multicell concentrating assembly (MCA) is explained in **Figure 2**. It can be seen that the design is based upon the Cassegrain arrangement of two parabolic concentrators, with the intention of achieving the area concentration. Such concentrating assembly acts as a collimating reflector where the parallel solar radiations are converted into concentrated collimated beam. Both parabolic reflectors are arranged such that their focal points coincide with each other. In addition, one of the reflectors uses its inner surface for reflection, while the other uses its outer surface. The primary reflector converges the incoming parallel rays at its focal point. However, these converging rays interact with the outer surface of secondary parabolic reflector which is placed in their way to the focal point. The secondary reflector introduces the cancelation effect which converges rays and diverges them as parallel rays. However, due to smaller contact surface of secondary reflector, the diverged collimated rays become concentrated before they hit the inlet aperture of homogenizer. In order to design multicell concentrating assembly (MCA), the edge ray is traced such that it hits point 'b' of secondary concentrator after being reflected by point 'a' of primary concentrator. As the foci of both reflectors are coinciding, therefore, the edge ray become parallel again after being reflected by the outer surface of secondary reflector and enter the homogenizer through its inlet aperture. This edge ray, after entering into the homogenizer, hits point 'c', which is located at its lower tapered portion. This lower tapered portion of multi-leg homogenizer is designed such that the edge ray, after being reflected by total internal reflection from point 'c', hits point 'e' of outlet aperture of homogenizer and falls on the MJC, placed there. The distribution of such parallel ray distribution is easily explained in simple schematic shown in **Figure 2(b)**. The back surface of MJC is attached to the heat spreader and heat sink assembly, to effectively dissipate the heat during CPV operation. It can be seen that the rays, after being reflected by secondary reflector, become concentrated over an area and size of such area concentration depends upon the size of secondary reflector.

There are three phases in which the design of proposed multicell concentrating assembly (MCA) is divided. The first phase is related to the calculations needed for the sizing of primary reflector. The main factor determining the size of primary reflector is the concentration requirement, depending upon the MJC specifications. The second phase is related to the form

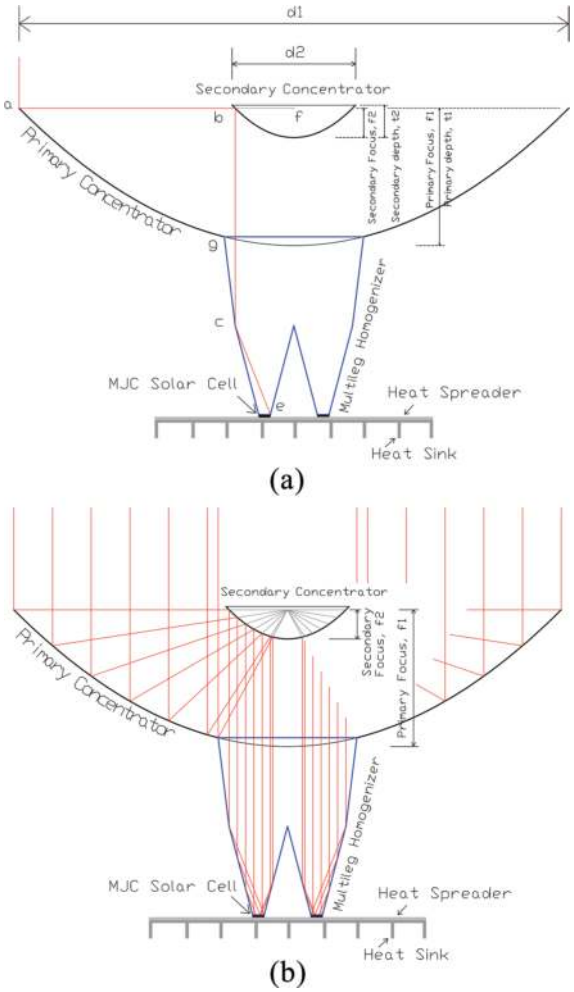

Figure 2. (a) Design and (b) ray distribution of proposed multicell concentrating assembly (MCA).

and the design of multi-leg homogenizer, which is also depending upon the specification of MJC as the outlet apertures of homogenizer must have dimensions same as MJC size. After finalizing the design of multi-leg homogenizer, the third phase is related to the secondary reflector sizing as it depends upon the size of inlet aperture of homogenizer. The detailed procedure associated with the overall design of multicell concentrating assembly (MCA) will be explained in this section.

The design parameters associated with the sizing of primary parabolic reflector are given in **Table 1**. It can be seen that the concentration ratio selected for the targeted prototype of MCA is 165, for the MJC of size (5.5 × 5.5 mm). Concentration ratio of 165 is only chosen to limit the overall size of the primary reflector due to budget limitations as larger reflector will cost

higher at the prototyping stage. Therefore, a reasonable concentration ratio of 165 is chosen to prove the concept. This concentration is only chosen for prototype design purpose, while the MCA can be designed for any concentration ratio of ×500 or ×1000, depending upon the specification of MJC. In order for the rays to enter homogenizer, a center hole of square size (50 × 50 mm) is cut in the primary parabolic reflector, as demonstrated in **Figure 3**.

From **Figure 3**, it can be seen that the effective area of MCA, to capture the solar radiations, is the one highlighted in white, which is calculated by Eqs. (1) and (2).

$$\text{Effective area of concentrating assembly } A_{CA} = CR_g \times A_M \times 4 \tag{1}$$

$$\text{Area of primary concentrator} = d_1^2 = A_{CA} + A_H \tag{2}$$

Parameter 'd' defines the dimension of square parabolic reflector. It must be noted that the square shape of primary reflector is firstly considered because of uniform distribution of

Sr. no.	Parameter	Symbol	Units	Value
1	Geometric concentration ratio	CR_g	—	165
2	Area of MJC	A_M	m^2	0.00003025 (5.5 × 5.5 mm)
3	Area of center square hole	A_H	m^2	0.0025 (50 × 50 mm)

Table 1. Primary reflector design parameters.

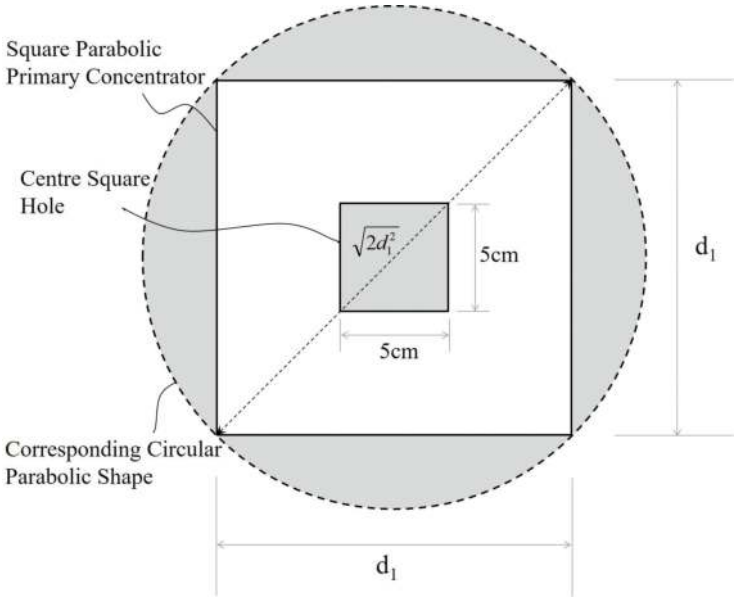

Figure 3. Simple schematic for primary reflector size calculations.

rays over cell area as MJC is of square shape. Secondly, the square shape primary reflector provides maximum packing density and perfect arrangement within CPV module, without leaving any empty pocket.

In Eq. (1), factor '4' is used because of four outlet apertures of homogenizer, with the size same as MJC. By using the concentration ratio of 164, the size of square primary parabolic reflector is calculated as 15 × 15 cm. Before proceeding to the design of multi-leg homogenizer, it is important to trace the position of edge ray. It must be noted that, as per **Figure 3**, the primary parabolic reflector is actually a square-cut piece of circular shape, and the diagonal of square reflector gives the diameter of the circular shape, as given by Eq. (3):

$$D_1 = \sqrt{d_1^2 + d_1^2} = \sqrt{2d_1^2} \tag{3}$$

Besides the size of primary reflector, it is also very important to keep the overall height of CPV modules minimum as it can make shipping and handling easy and cheap. It can also lessen the mechanical problems faced during CPV operation. Therefore, in order to keep the overall height of MCA minimum, the focal point of primary parabolic reflector is kept same as its depth 't'. By using the parabolic curve equation, the focal point 'f_1' of primary parabolic concentrator can be calculated by Eq. (4):

$$f_1 = \frac{(D_1/2)^2}{4t_1} = \frac{D_1^2}{16f_1} \quad (f_1 = t_1) f_1^2 = \frac{D_1^2}{16} \tag{4}$$

Diameter 'D_1' of corresponding circular shape of primary reflector can be calculated as 21.2132 cm, by using the 15 cm size in Eq. (3). As a result, Eq. (4) gives the focal point value of primary parabolic concentrator as 5.3033 cm. The simple parabolic Eq. (5) can now be used to calculate the coordinates of the parabolic surface of primary reflector:

$$x^2 = 4fy \tag{5}$$

The multi-leg homogenizer is consisting of four similar sections, joined together as a single unit. Therefore, for easy understanding, the design of single section will be explained in detail first, which will be combined together to form the proposed multi-leg homogenizer. The simple 2D schematic of multi-leg homogenizer is shown in **Figure 4** where only its two sections are shown. Each single section of multi-leg homogenizer has two tapered section, i.e., above and below line 'eb'. The tapered section below line 'eb' is designed such that it uniformly distributes solar radiations over the cell area in case of parallel rays. However, the tapered section above line 'eb' is designed to accommodate the tracking error by guiding the non-parallel incoming solar radiations towards the outlet aperture of homogenizer. In order to discuss the homogenizer design, it is better to discuss the case for parallel rays first, for easy understanding.

Edge ray 'j' which is parallel to the primary reflector axis, as shown in **Figure 4**, is the same edge ray explained in **Figure 2(a)** that is coming from secondary reflector. However, after entering into the homogenizer, it hits point 'b' located at the start of lowered tapered portion

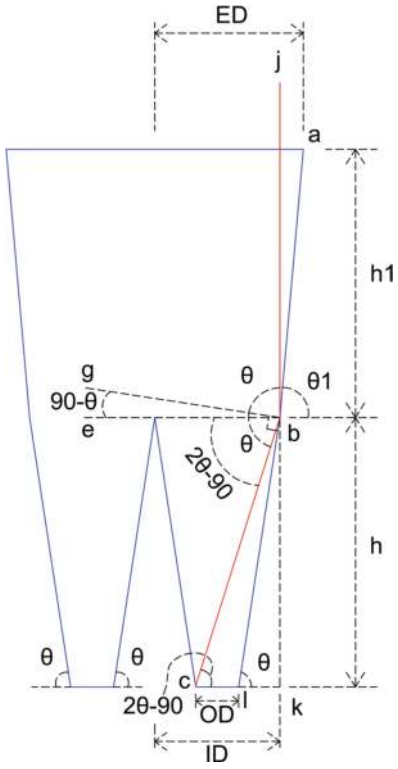

Figure 4. Multi-leg homogenizer design and schematic.

of homogenizer. Such a ray must exit through edge point 'c' of the outlet aperture of the homogenizer, to ensure uniform distribution of solar radiations over the cell area. Therefore, the dimensional parameters of lower tapered portion of homogenizer, i.e., height 'h' and slope angle 'θ' of side line 'bl', are of prime importance here. As explained, the value of these two parameters must be tuned such that the parallel edge rays, after passing through the homogenizer, must exit through end point 'c' of outlet aperture. **Figure 4** shows the angular position of such tapered portions as defined by the trigonometric laws. The angle between line 'bl' and the hypothetical line 'bg' is taken as 'θ'. As these lines are perpendicular to each other, therefore, the edge ray also makes same angle 'θ' with the hypothetical line 'bg'. By considering the triangular section Δckb, the height 'h' of lower tapered portion of homogenizer is given by Eq. (6):

$$h = \left[OD + \left(\frac{ID - OD}{2}\right)\right].\tan(2\theta - 90) \tag{6}$$

It can be seen that there are two unknowns in Eq. (6), i.e., 'θ' and 'h'. Therefore, such equation cannot be solved for the mentioned unknowns. For the solution of such equation, the triangle Δblk can be considered to get Eq. (7):

$$h = \left(\frac{ID - OD}{2}\right).\tan\theta \tag{7}$$

If Eqs. (6) and (7) are compared, then we can find the expression for the lower slope angle 'θ' as given by Eq. (8):

$$\left[OD + \left(\frac{ID - OD}{2}\right)\right].\tan(2\theta - 90) = \left(\frac{ID - OD}{2}\right).\tan\theta \tag{8}$$

Parameter 'OD' represents the dimension for the outlet aperture of homogenizer, which is same as the size of MJC, i.e., 5.5 mm. On the other hand, a suitable value of '16' is also considered for parameter 'ID' so that ray can easily be propagated to the outlet aperture. If the value of 'ID' is small, then the height 'h' will also be small, same for 'OD'. Otherwise, the ray will have multiple total internal reflections (TIR) inside the homogenizer if the value of 'h' is higher for smaller 'ID'. Or, there may be a chance that the ray can propagate back if the value of 'h' is very big. However, the large value of 'ID' also requires a larger value of 'h', same for 'OD'. For the given value of 'ID' and 'OD', the value of 'θ' and 'h' can be calculated as 81.33° and 34.43 mm, respectively.

After finalizing the design of lower tapered portion of the homogenizer, now the upper tapered portion of homogenizer is considered, which is needed to be designed to accommodate the rays which are not parallel to the axis of concentrating assembly. From the design point of view, a tracking error of 1° is selected which can be handled by the homogenizer. This means that the homogenizer design will be able to handle the deviated ray for maximum angle of 1°. By using the graphical method and trigonometric laws, it has been shown in **Figure 5** that if there

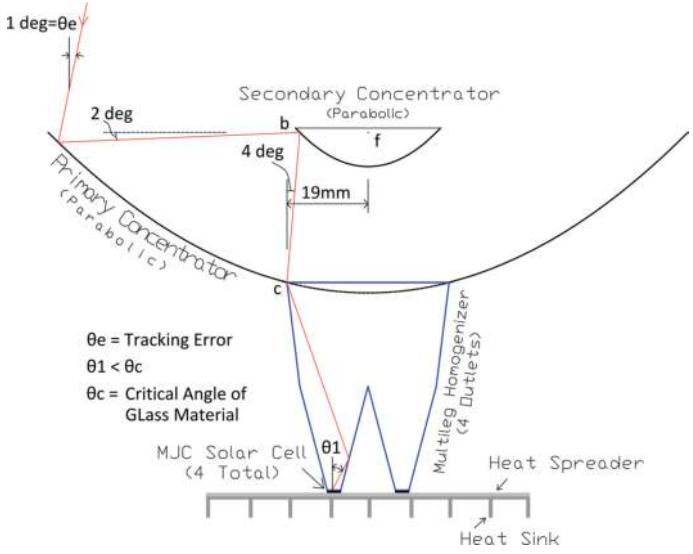

Figure 5. Acceptance angle calculation for multicell concentrating assembly.

is 1° deviation in the incident ray from the primary reflector axis, such deviation increases to 2° after being reflected by the primary reflector. Similarly, after being reflected by secondary reflector, this deviation increases to 4°. Therefore, to handle such 1° deviation in the incident ray, by the homogenizer, its half width is found to be 19 mm, by the graphical method.

In the third phase of MCA design, the size of secondary reflector is calculated. As shown in **Figure 2(A)**, the edge ray, after being reflected by point 'b' of secondary reflector, hits point 'c' of the homogenizer which is the edge point of lower tapered portion of 'ID'. Therefore, for the calculation of the focal point of secondary reflector, the value of D_1 = ID should be used in Eq. (4). The main reason for this consideration is that the focal point of both reflectors is coinciding as the parallel ray pattern is needed to be achieved after secondary reflection, which must hit the lower tapered portion of the homogenizer with size 'ID = 16 mm'. However, the radius of secondary reflector will be according to 'ED' which is found to be '19 mm'. The coordinates for parabolic surface of secondary reflector can be found using Eq. (5), for the value of 'x' being varied from 0 to 19. The size of secondary reflector is same as that of the inlet aperture of the homogenizer, to account for the tracking error.

4. Development of MCA-based CPV prototype

To verify and analyze the field performance of proposed and designed MCA, a prototype of CPV is fabricated as per designed concentration ratio of ×165. The prototype of fabricated MCA is shown in **Figure 6** and the MCA-based novel CPV unit is shown in **Figure 7**. The primary and secondary reflectors are machined from aluminum blocks. However, to improve the surface quality and reflection characteristics, the reflecting surface of both reflectors was coated with thin optical graded reflecting aluminum layer, using sputter-coating method. The multi-leg homogenizer was fabricated in the form of four symmetrical pieces which were joined together to form a single unit. Each homogenizer piece is similar to the half of schematic shown in **Figure 4**. The individual pieces of homogenizer were machined using N-BK7 glass material. To form a single homogenizer unit, all four pieces were joined together using optical graded UV glue. It must be noted that the machining method of fabrication is an expensive fabrication technique, and that is why smaller concentration ratio was chosen at the start to keep the overall cost minimum. However, for mass production of reflectors and homogenizers, injection molding techniques for plastic and glass materials are used.

Four MJCs were attached at the four outlet apertures of the homogenizer. However, the back side of MJCs was attached to the heat spreader and heat sink to dissipate the heat during CPV operation and to keep the cell temperature within optimum limit.

In order to test the performance of developed novel MCA-based CPV module, a two-axis solar tracking unit was used with tracking accuracy of 0.1° [20, 21]. The developed CPV module was mounted onto the top frame of solar tracker. The tracking system is based upon the hybrid tracking algorithm which defines the solar position through both active and passive techniques. After calculating the position of sun, based upon the solar geometry model, the actual position of the sun is verified by taking the real-time feedback

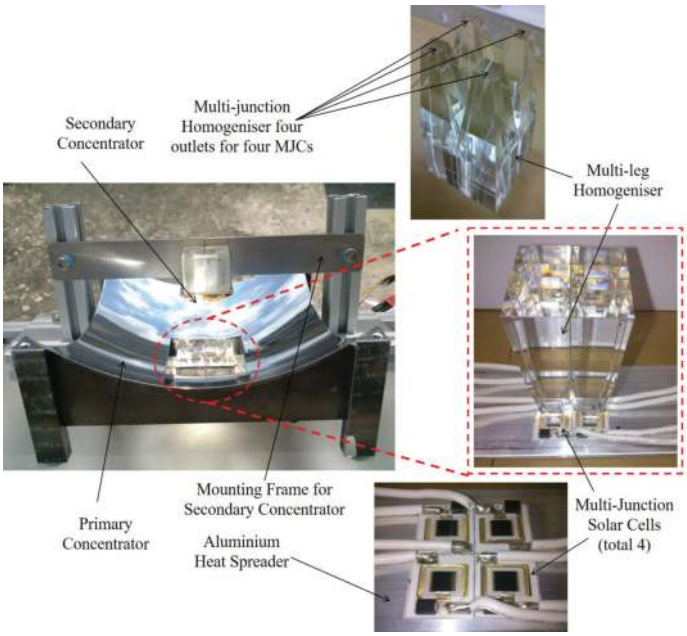

Figure 6. Developed prototype of multicell concentrating assembly (MCA)-based CPV module.

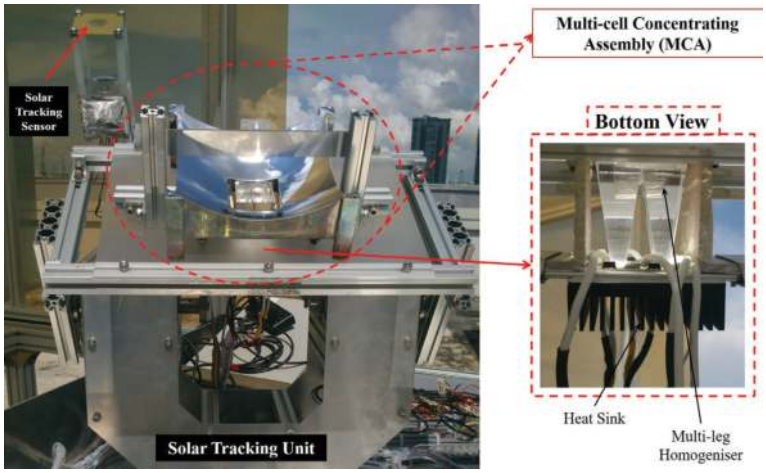

Figure 7. Experimental prototype of MCA-based novel CPV unit.

from solar tracking sensor. Such real-time optical feedback avoids any chance of tracking error which may arise due to passive tracking method and possible backlash in the driving assembly.

5. Results and discussion

In order to analyze the optical performance of proposed multicell concentrating assembly (MCA), the ray tracing simulation was conducted using TracePro software. The concentrating assembly was analyzed in terms of division of rays among four outlet apertures, uniformity of rays at the outlet aperture and investigation of deflected path of incident rays. The simulation model for proposed MCA, according to the discussed design, is shown in **Figure 8**. To conduct ray tracing simulation, a square grid of parallel rays was selected as the primary reflector is also of square shape. As the received solar radiation is not exactly parallel in nature, that is why the simulated MCA model was not only investigated for parallel ray grid but also for the grid with angle same as the solar subtended angle. The ray tracing simulation results of proposed MCA design with parallel ray grid are shown in **Figure 9**. It can be seen that a perfect division of rays among four outlet apertures of homogenizer is experienced. In addition, the rays are also uniformly distributed over the whole surface area of outlet aperture. Moreover, a concentrated collimated beam is also achieved after reflection of parallel incident rays from secondary reflector. As per discussed design, this concentrated collimated beam is being divided among four sections of homogenizer and also hitting the lower tapered portion of the homogenizer.

In order to simulate the optical performance of proposed MCA in real field environment, the simulation results for grid of rays with solar subtended angle are shown in **Figure 10**. These rays are not exactly parallel to the axis of primary reflector but have a small deviation which is same as the actual solar radiations, received during real field operation. It can be seen that there is still a perfect division of received radiations among four sections of the homogenizer and uniform distribution of these radiations over the outlet apertures of homogenizer. However, one of the differences which can be seen here is that the rays are also hitting the upper tapered portion of the homogenizer, without any induced ray deviation. The reason

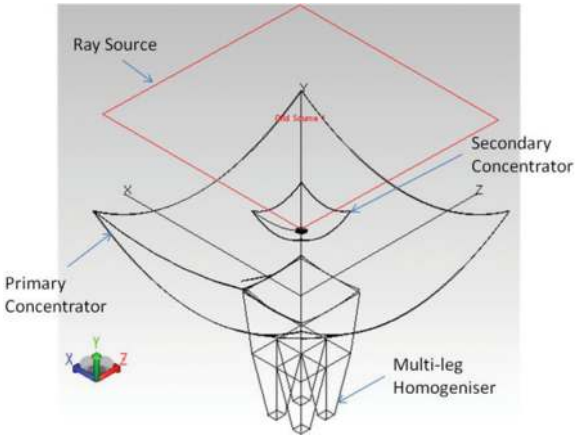

Figure 8. TracePro model of multicell concentrating assembly (MCA) for ray tracing simulation.

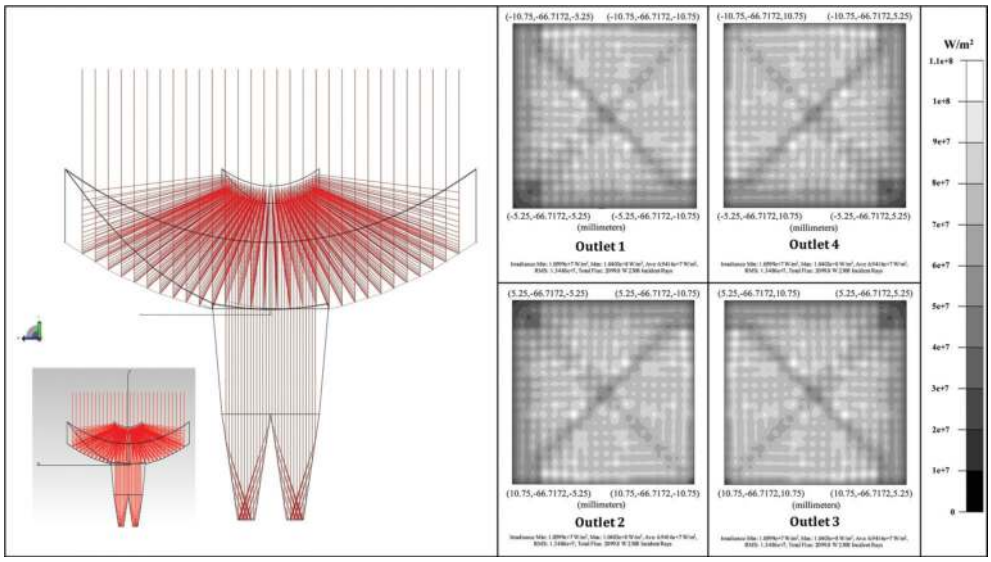

Figure 9. Ray tracing simulation of multicell concentrating assembly for parallel rays.

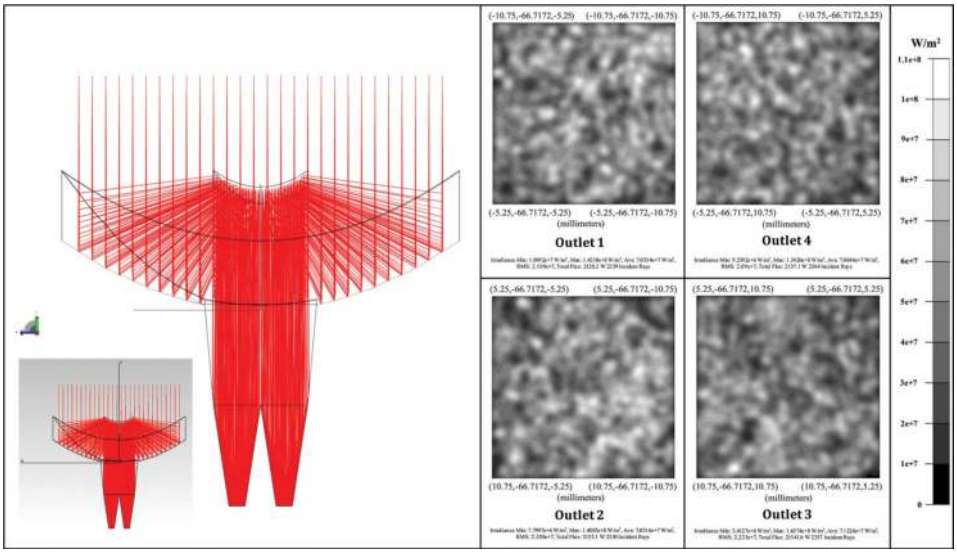

Figure 10. Ray tracing simulation of multicell concentrating assembly for solar subtended angle.

is that the incoming rays are already not parallel to the axis of primary reflector, and that is why they are reflected by the upper tapered portion which is designed to accommodate the tracking error or rays which are not parallel to the primary reflector axis.

After verifying the design of developed multicell concentrating assembly (MCA) through ray tracing simulation, it is also important to verify its performance under real conditions during field testing. The developed prototype of CPV system, with MCA-based design, was tested under field condition, and the output from each of the MJC, at four outlet apertures of homogenizer, was logged in real time using data logging unit. The power and voltage output of each of four MJCs is shown in **Figures 11** and **12**. From both figures, it is clear that there is equal distribution of solar radiations among four MJCs, during whole-day operation as their power and voltage plot look similar. It must be noted that the solar tracking unit was operated with tracking accuracy of 0.3°, instead of 0.1°. The equal output of all four MJCs, with such tracking accuracy, verifies the proposed design of multicell concentrating assembly (MCA) and its compatibility in fulfilling the objective.

Another important test to investigate the response of concentrating assembly against different angular deviations of incident rays is expressed in the form of normalized power curve. So far, the performance of MCA, either simulated or experimental, is tested for parallel rays or rays with smaller deviations. In order to test the maximum response limit of concentrating assembly over different deviation angles, the normalized power output of the system is plotted against the angular deviation. Such normalized power curve also helps to predict the acceptance angle of concentrating assembly for efficient operation. The normalized power curve for developed multicell concentrating assembly (MCA)-based CPV is shown in **Figure 13**. The red line indicates the normalized power curve obtained from ray tracing simulation against different deviation angles of parallel rays. The simulated normalized power is obtained by taking the ratio of the total number of rays at the outlet apertures to the total incident rays. However, the blue line indicates the true normalized power output curve obtained through

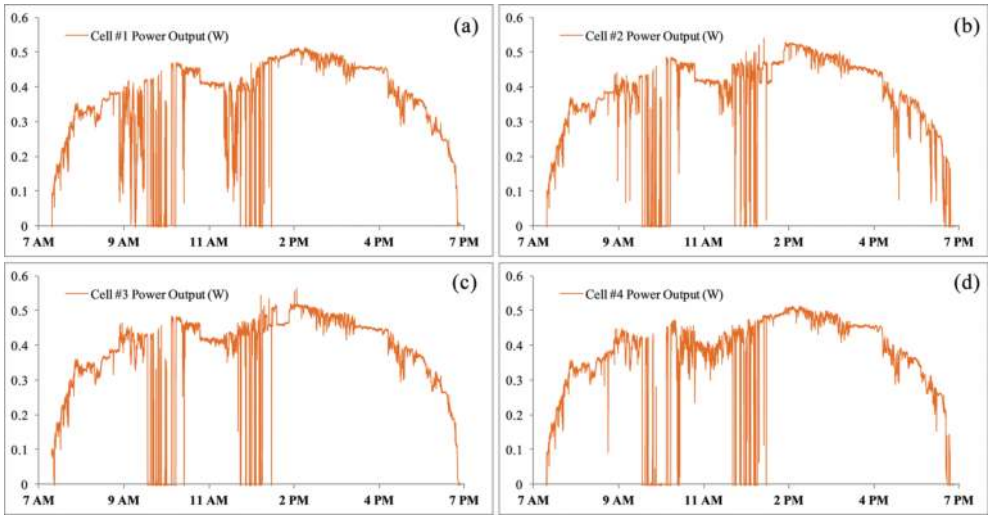

Figure 11. Power output for individual cell of MCA-based CPV system.

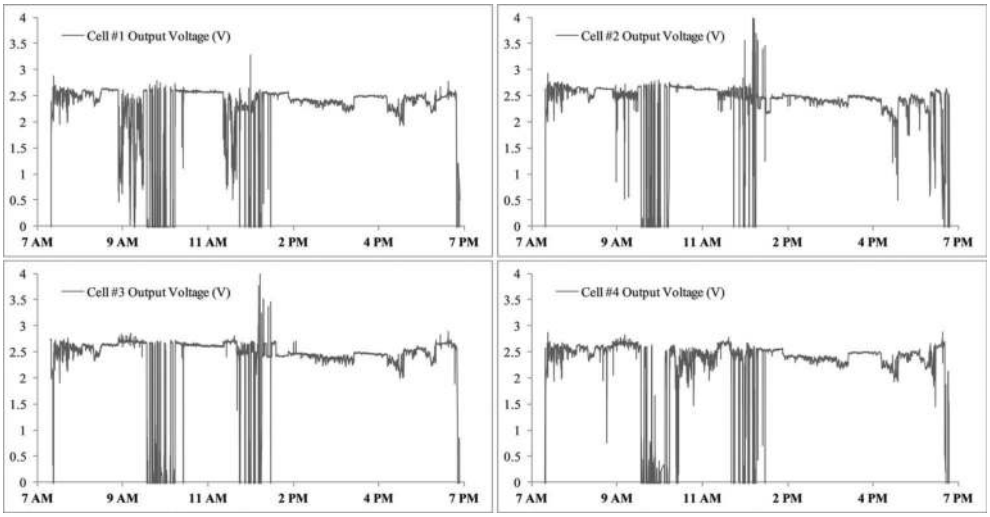

Figure 12. Voltage output for individual cell of MCA-based CPV system.

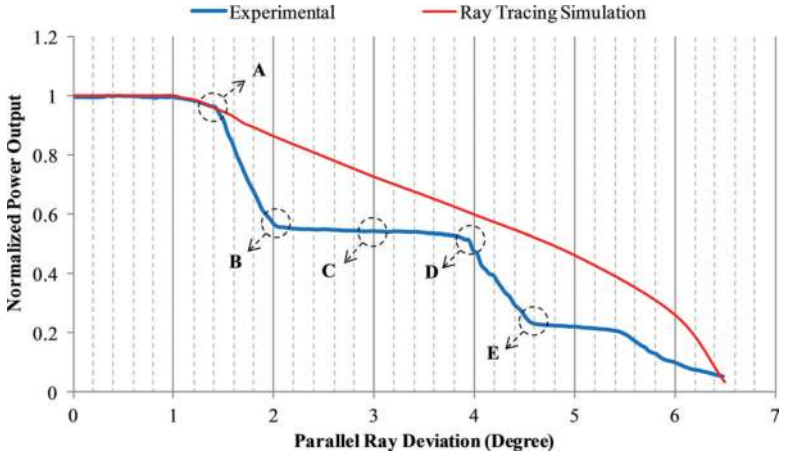

Figure 13. Normalized power curves for multicell concentrating assembly-based CPV system.

experimentation. In order to obtain such plot, the tracker movement was stopped, while the CPV module was exactly facing the sun, during noontime. The angular deviation was calculated by taking the difference in the initial and current position of sun. The power output of all four MJCs, connected in series, was logged under real time for constant output load. It is clear from **Figure 13** that the simulated normalized power output is almost 100% for angular deviations up to 1°. It is also true for experimental results, which verifies the proposed design of MCA. If there is further increase in the incident ray deviation, than 1°, the normalized power starts to drop.

It can be seen that there is a good agreement between simulated and experimental normalized power curves, until point 'A'. However, the experimental curve starts deviating from simulated curve after point 'A'. There is gradual decrease in the simulated power curve. However, a stepwise drop is observed for experimental curve. Such a different response of simulated

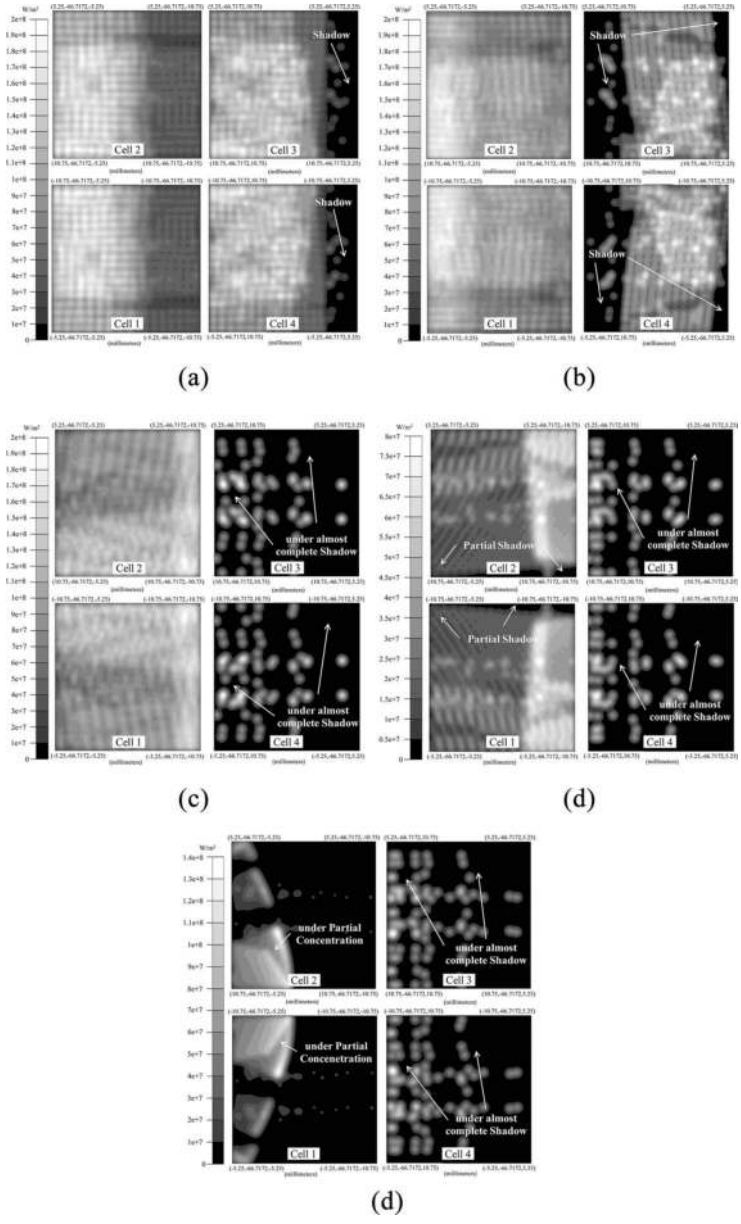

Figure 14. Simulated irradiance map at outlet apertures of multi-leg homogenizer for different angular deviations of parallel rays.

and experimental normalized power curves can be explained with the fact that the simulated power output is just based upon the number of radiation received at the outlet apertures of homogenizer. However, for experimental curve, the power output is the actual electrical power obtained from CPV module but at a constant load. As the load across CPV module is constant, therefore, excessive ray loss causes its maximum power point to shift, resulting in a decrease in its output and performance. That is why it also deviates from the simulated curve. To carefully understand the varying trend of simulated and experimental normalized power curves, the simulated irradiance map at all four outlet apertures of homogenizer is shown in **Figure 14**. The irradiance maps are plotted against different points mentioned on experimental normalized curve. It can be seen from **Figure 14(A)**, which shows the irradiance map at point 'A', that the solar cells 3 and 4 are coming under shadow. For simulated curve, this shadow is just a decrease in the number of rays coming out of the homogenizer. However, in actual system, the electrical output of the CPV system is greatly disturbed as all MJCs are connected in series. The maximum power point for cells under shadow changes, and they also pulls down the performance of other MJCs due to their series connection. Therefore, overall electrical output of complete CPV module decreases. At points 'B', 'C' and 'D', the normalized electrical power output of CPV system is almost same as 50%. This is because of the fact that at this point, only two cells are operating, while the other two cells are under complete shadow, as shown in **Figure 14(B)–(D)**. However, for simulated power curve, there is still a gradual decrease for these points which implies that the net flux output is not reduced to 50% for all these three points, i.e., 'B', 'C' and 'D'. The main reason for half of electrical output is because of the shift in the maximum power point for the entire CPV system, which is effected by the two cells under shadow.

After increasing deviation angle beyond point 'D', the experimental curve again starts to drop till point 'E'. This is because of the fact that now the other two cells are also coming under shadow, as can be seen in **Figure 14(D)**. At point 'E', the remaining two cells are under only partial concentration. That is why the power output reduced to a low value. The power output remains stable for a while after point 'E' which is just because of partial concentration that moves around the cell area due to leftover and scattered radiations. With further increase in the deviation angle, the power output slowly dies to zero. The normalized power output curve shows that the develop CPV system, based upon the proposed MCA, has acceptance angle of 1° as designed. However, it has a capability of operation for deviation angle as high as 6.5°. However, the power output drops significantly, but the system can still respond to the received radiations.

6. Summary of the chapter

In the current photovoltaic market, with dominating share of single-junction solar cells, the highly efficient concentrated photovoltaic systems (CPV), utilizing third-generation multi-junction solar cells, have yet to exploit their market potential due to their design complexities. The conventional CPV module design utilizes individual concentrator for each MJC. This chapter has introduced a novel design of CPV concentrating assembly where single

concentrator can handle four MJCs, named as multicell concentrating assembly (MCA). Such proposed design will not only reduce the overall cost of the system, but it will also reduce the assembly and alignment efforts during CPV module fabrication.

In this chapter, a detailed design of such multicell concentrating assembly is discussed and explained. For prototype purpose, the detailed calculation of concentrating assembly size is presented for concentration ratio of ×165. Such proposed design is transformed into working prototype of CPV module for actual field testing. The design was targeted to handle angular deviations of 1° without any loss in performance.

A detailed performance investigation strategy was adopted to verify the proposed design with its prototype and its limitation during field operation. An optical simulation was conduction in TracePro to verify the optical performance of MCA. An equal division and uniform distribution of rays were observed at the outlet apertures of homogenizer. From the field testing, equal and uniform power output of each MJC verified the proposed design of multicell concentrating. However, to analyze the response of MCA against angular deviation of incident ray, normalized power output curve was presented against angular deviation, for both experimental and simulated performances. The system showed 100% power output for angular deviations up to 1°, as designed. However, the system showed maximum capability of handling 6.5° angular deviations. A great agreement was observed among simulated and experimental results.

Nomenclature

d_1	dimension of square primary reflector of multi-leg homogenizer concentrating assembly (mm)
t_1	depth of primary reflector of multi-leg homogenizer concentrating assembly (mm)
f_1	focal length of primary reflector of multi-leg homogenizer concentrating assembly (mm)
A_M	area of multi-junction solar cell (mm^2)
D_1	corresponding diameter of primary reflector of multi-leg homogenizer concentrating assembly (mm)
θ_e	tracking error (degree)
CR_g	geometric concentration ratio
d_2	dimension of square secondary reflector of multi-leg homogenizer concentrating assembly (mm)
t_2	depth of secondary reflector of multi-leg homogenizer concentrating assembly (mm)
f_2	focal length of secondary reflector of multi-leg homogenizer concentrating assembly (mm)
A_{CA}	area of concentrating assembly (mm^2)

A_H area of center hole in primary reflector of multi-leg homogenizer concentrating assembly (mm^2)

θ_c critical angle of glass material (degree)

MJC multi-junction solar cell

Author details

Muhammad Burhan*, Muhammad Wakil Shahzad and Kim Choon Ng

*Address all correspondence to: muhammad.burhan@kaust.edu.sa

Water Desalination and Reuse Centre, Biological and Environmental Science and Engineering Division, King Abdullah University of Science and Technology, Saudi Arabia

References

[1] Najibi F, Niknam T. Stochastic scheduling of renewable micro-grids considering photovoltaic source uncertainties. Energy Conversion and Management. 2015;**98**:484-499

[2] Burhan M, Shahzad MW, Ng KC. Development of performance model and optimization strategy for standalone operation of CPV-hydrogen system utilizing multi-junction solar cell. International Journal of Hydrogen Energy. 2017;**42**(43):26789-26803

[3] Burhan M, Chua KJE, Ng KC. Electrical rating of concentrated photovoltaic (CPV) systems: Long-term performance analysis and comparison to conventional PV systems. International Journal of Technology. 2016;**7**(2):189-196. DOI: 10.14716/ijtech.v7i2.2983

[4] Ng KC, Burhan M, Shahzad MW, Ismail AB. A universal isotherm model to capture adsorption uptake and energy distribution of porous heterogeneous surface. Scientific Reports. 2017;**7**(1):10634

[5] Burhan M, Chua KJE, Ng KC. Sunlight to hydrogen conversion: Design optimization and energy management of concentrated photovoltaic (CPV-hydrogen) system using micro genetic algorithm. Energy. 2016;**99**:115-128

[6] Chantana J, Ueno S, Ota Y, Nishioka K, Minemoto T. Uniqueness verification of direct solar spectral index for estimating outdoor performance of concentrator photovoltaic systems. Renewable Energy. 2015;**75**:762-766

[7] Burhan M, Oh SJ, Chua KJE, Ng KC. Double lens collimator solar feedback sensor and master slave configuration: Development of compact and low cost two axis solar tracking system for CPV applications. Solar Energy. 2016;**137**:352-363

[8] Burhan M, Oh SJ, Chua KJ, Ng KC. Solar to hydrogen: Compact and cost effective CPV field for rooftop operation and hydrogen production. Applied Energy. 2017;**194**:255-266

[9] Burhan M, Shahzad MW, Ng KC. Long-term performance potential of concentrated photovoltaic (CPV) systems. Energy Conversion and Management. 2017;**148**:90-99

[10] Shockley W, Queisser HJ. Detailed balance limit of efficiency of p-n junction solar cells. Journal of Applied Physics. 1961;**32**(3):510-519

[11] Burhan M, Shahzad MW, Choon NK. Hydrogen at the rooftop: Compact CPV-hydrogen system to convert sunlight to hydrogen. Applied Thermal Engineering. 2018;**132**:154-164

[12] Burhan M, Chua KJE, Ng KC. Long term hydrogen production potential of concentrated photovoltaic (CPV) system in tropical weather of Singapore. International Journal of Hydrogen Energy. 2016;**41**(38):16729-16742

[13] Baig H, Sellami N, Mallick TK. Trapping light escaping from the edges of the optical element in a concentrating photovoltaic system. Energy Conversion and Management. 2015;**90**:238-246

[14] Burhan M, Chua KJE, Ng KC. Simulation and development of a multi-leg homogeniser concentrating assembly for concentrated photovoltaic (CPV) system with electrical rating analysis. Energy Conversion and Management. 2016;**116**:58-71

[15] Wang C, Abdul-Rahman H, Rao SP. A new design of luminescent solar concentrator and its trial run. International Journal of Energy Research. 2010;**34**(15):1372-1385

[16] Muhammad B, Seung JO, Ng KC, Chun W. Experimental investigation of multijunction solar cell using two axis solar tracker. Applied Mechanics and Materials. 2016;**819**: 536-540. Trans Tech Publications

[17] Burhan M, Shahzad MW, Oh SJ, Ng KC. A pathway for sustainable conversion of sunlight to hydrogen using proposed compact CPV system. Energy Conversion and Management. 2018;**165**:102-112

[18] Garboushian V, Stone KW, Slade A. The Amonix high-concentration photovoltaic system. Concentrator Photovoltaics. 2007;**130**:253

[19] Burhan M, Shahzad MW, Ng KC. Sustainable cooling with hybrid concentrated photovoltaic thermal (CPVT) system and hydrogen energy storage. International Journal of Computational Physics Series. 2018;**1**(2):40-51

[20] Oh SJ, Burhan M, Ng KC, Kim Y, Chun W. Development and performance analysis of a two-axis solar tracker for concentrated photovoltaics. International Journal of Energy Research. 2015;**39**(7):965-976

[21] Burhan M. Theoretical and Experimental Study of Concentrated Photovoltaic (CPV) System with Hydrogen Production as Energy Storage (Doctoral Dissertation); 2015